전기자동차용 3kW급 LDC를 위한 통합형 플라나변압기 설계

라마단[1], 석채영[1], 김상진[1], 최세완[1], 유병우[2], 박상훈[2]
서울과학기술대학교[1], LG전자[2]

Integrated Planar Transformer Design of 3 kW LDC for Electric Vehicles

Ramadhan[1], Chaeyoung Suk[1], Sangjin Kim[1], Sewan Choi[1],
Byeongu Yu[2], Sanghun Park[2]
Seoul National University of Science and Technology[1], LG Electronics[2]

ABSTRACT

Abstract—This paper presents an optimal planar transformer design of a 3-kW Low voltage DC-DC Converter (LDC) with 3.68 kW/L power density for electric vehicle (xEV) application. The transformer is optimized based on the trade-off between footprint and loss using the proposed figure-of-merit (FOM) based optimization. In order to achieve ZVS under entire load range, an external leakage inductance is added and implemented using the proposed magnetic integration technique. A comparison between non-integrated and integrated magnetic core using finite element analysis (FEA) is presented. The result shows that the integrated core can reduce the core loss up to 35 % and core boxed volume up to 15 % compared to the non-integrated core. Experimental results are also provided to validate the proposed magnetic integration technique.

1. Introduction

Electric vehicles (xEVs) are gaining more attention and popularity due to its competitiveness with internal combustion engine vehicles and its low greenhouse gas emission. LDC is one of the key components in xEV's electrical system that functions as an interface between the high voltage battery (240 V ~ 440 V) to the low voltage battery (11.5 V ~ 15.5 V). This low voltage battery supplies the xEV's auxiliary loads such as power window, lamps, instrument panel and in-car entertainments [1].

Phase shift full bridge converters have been widely implemented in electric vehicle application due to its desirable characteristics such as wide range ZVS operation of all primary switches by using the leakage and magnetizing inductance of the transformer, and output capacitances of the switches [2]. For low voltage high current rectifier side, the current doubler topology is preferred. In current doubler rectifier, the secondary winding of the transformer only carries half of the output current at a time, resulting in lower winding current rating [3]. In this paper, the primary switches are implemented using SiC MOSFET with 250 kHz switching frequency. To achieve high efficiency, SR switch is utilized in the low voltage side, instead of diode rectifier. The phase shift full bridge topology with current doubler rectifier is shown in Fig. 1.

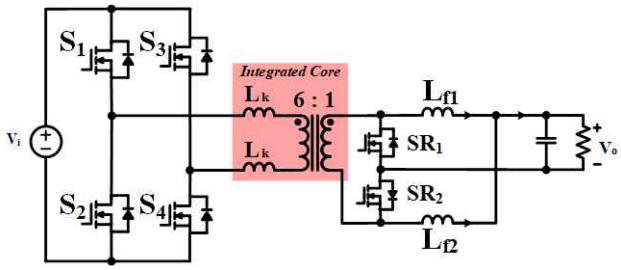

Fig. 1 PSFB Converter with proposed integrated magnetic structure

As mentioned in the previous section, the ZVS operation of the primary switches in PSFB converter relies on the energy stored in the leakage inductance. However, due to the winding interleaving arrangement of the transformer which is commonly employed to reduce the ac resistance, the leakage inductance of the planar transformer might be too small for the required ZVS operation. In this paper, an integration technique between leakage inductor and transformer is proposed. Also, a transformer optimal design based on the proposed figure-of-merit (FOM) method is presented.

2. Optimal Design of Integrated Planar Transformer

This section describes the transformer optimization method based on figure-of-merit (FoM). The objective of the optimization is to select core maximum flux density (B_{max}) and winding current density (J) based on the tradeoff between footprint and loss. These two objective functions can be simplified using the proposed figure-of merit method which is defined as,

$$FoM = fp.P_{loss} \quad (1)$$

where fp represents the total footprint of the transformer while P_{loss} is the total of the transformer core loss and winding loss. P_{loss} and fp are functions of the core and

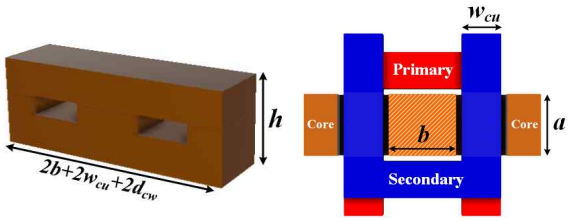

(a) (b)

Fig. 2 (a) Transformer core dimensions (b) Top view of core and winding dimensions (omitted upper part)

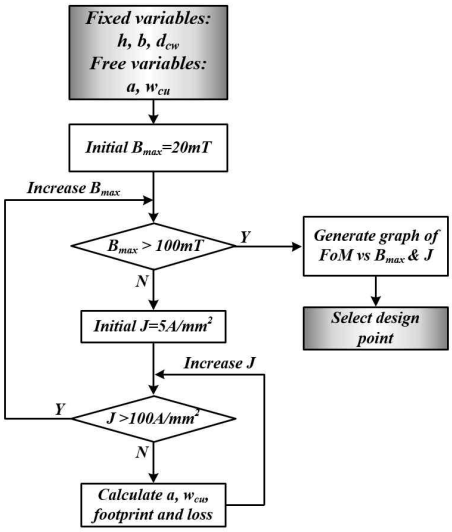

Fig. 3. Flowchart of the Figure-of-Merit based optimization

winding geometries as illustrated in Fig .2. Using the relationships in (2) and (3), B_{max} and J can be varied following the optimization flowchart shown in Fig. 3.

$$B_{\max} = \frac{v_{pri}.D}{2.(a.b).N_{pri}.f_s} \quad (2)$$

$$J = \frac{I_{pri}}{w_{cu}.t_{cu}} \quad (3)$$

A 3d graph is plotted in Fig 4. to visualize the relationship between B_{max}, J and FoM. The boundaries of the graph are obtained based on the defined footprint and loss constraints. Finally, the optimal design point can be selected from the global minimum of the graph which, in this case, corresponds to J=20A/mm^2 and B_{max}=0.08 T.

Due to the interleaving configuration of the transformer winding, the intrinsic leakage inductance of the transformer is very small, and its value is unpredictable. In this paper, the required leakage inductance is implemented by placing an additional core in series with the transformer. Fig. 5(a) shows the conventional way to put an additional inductor in series with transformer. The core and winding turns of the leakage inductor will increase the total footprint area. By using the extended primary winding as the leakage inductor turns, the footprint can be reduced as depicted in Fig. 5(b). To further reduce the footprint area without compromising the effective core cross sectional area of the inductor (A_e), an integration method between transformer and leakage

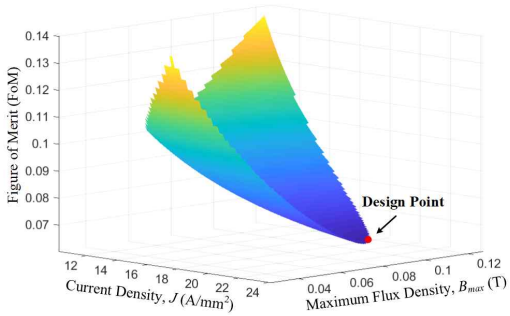

Fig. 4 FoM vs B_{max} and J

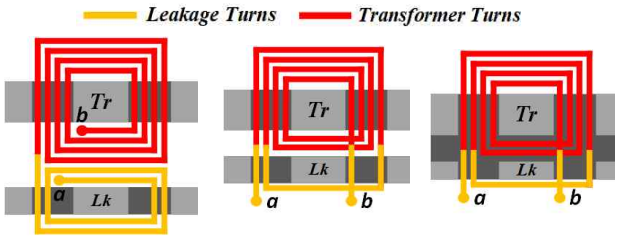

(a) (b) (c)

Fig. 5. Transformer and leakage inductor integration steps (a) conventional series inductor winding method (b) improved total footprint by winding integration (c) Integration by extending core plates

inductor is proposed. As depicted in Fig. 5(c). the core plates of the leakage inductor is extended so that it is connected to the transformer core. By doing this, A_e will increase since the flux generated by the leakage inductor is shared with the transformer. To maintain A_e, the leakage core cross sectional area can be reduced, resulting in smaller footprint area. Around 15% of boxed volume reduction can be expected by using this method

3. 3D Simulation FEA Analysis

A 3D FEA simulation using Ansys Maxwell was carried out. As shown in Fig. 4. in the integrated structure, the flux

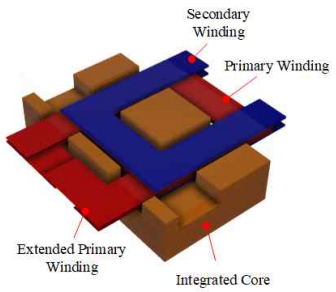

Fig. 6. 3D drawing of integrated magnetic structure

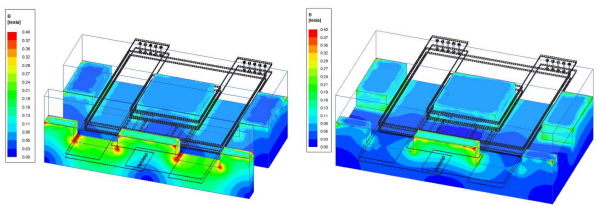

(b) (c)

Fig. 7. Flux density plot from FEA simulation (a) non-integrated (b) integrated

density of the leakage outer legs is much lower than that of the non-integrated structure. It can also be seen in the figure that the flux density of the transformer outer legs is slightly increased because of the flux addition from the leakage inductor. Despite of this increase in transformer flux density, the reduction in the leakage outer legs still contributes to a significant decrease in core loss. The core loss of the leakage inductor in the non-integrated structure is 14 W while the transformer is 8.5 W, yielding a total core loss of 22.5 W. Meanwhile, the integrated structure has a total core loss of 14.7 W. Since both structures have the same winding configuration their winding losses are the same.

4. Experiment Result

A 3-kW PSFB converter prototype was built in order to verify the performance of the proposed integrated magnetic structure. The input voltage is 240 V while the output voltage is 13.8 V. The magnetic components including the filter inductors are placed in a separate PCB stack as shown in Fig. 8.

For comparison purpose, another magnetic structure with separated leakage inductance was also built. Both structures are compared based on their temperature under the same condition. As can be seen in Fig. 9(a), in the non-integrated structure, the heat is concentrated in the leakage inductor core. The maximum heat of the leakage core reached 98°C. In contrast with the non-integrated structure, the heat generated by the core is distributed throughout the transformer and leakage inductor as shown in Fig. 9(b). In this structure the maximum temperature inside the core reached 65.8°C.

Fig. 10 shows the experimental waveform of the converter at boundary conduction mode (BCM) and full load condition. Under the BCM mode, the lagging leg switches

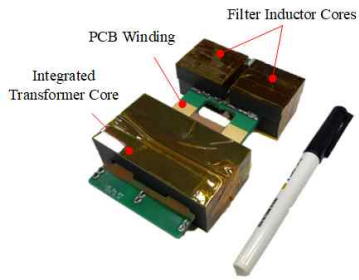

Fig. 8. Magnetic components with PCB winding structure

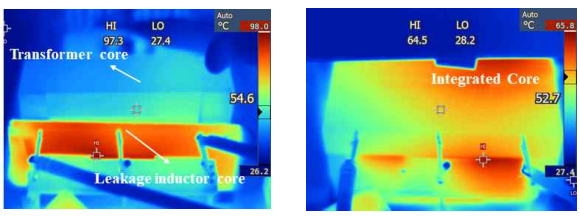

(a) (b)

Fig. 9 Core thermal image (a) non-integrated (b) integrated

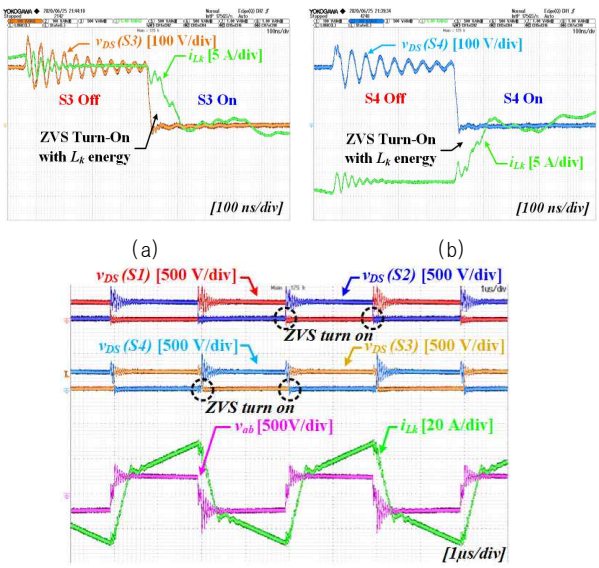

(a) (b)

(c)

Fig. 10 Experimental waveform at Vin = 240 V, Vo = 13.8 V
(a) Lagging leg switches transition under BCM (Po = 935 W)
(b) Experimental waveform at full load

(S3 and S4) rely solely on leakage inductance current to achieve ZVS. As can be observed in the waveform, S3 and S4 achieve ZVS under BCM.. Since the ZVS turn-on operation of the leading leg switches (S1 and S2) relies also on the load current (*Io*), its operation is guaranteed as long as the lagging leg switches can achieve ZVS.

5. Conclusion

An integrated planar magnetic structure between leakage inductor and transformer has been proposed for EV LDC. The proposed structure can achieve 35 % lower core loss compared to the non-integrated structure with the same footprint area. Experiment results show that the integrated core has lower core temperature. Based on the experimental waveform, the switches can achieve ZVS under the entire load range.

References

[1] S. M. N. Hasan, M. N. Anwar, M. Teimorzadeh and D. P. Tasky, "Features and challenges for Auxiliary Power Module (APM) design for hybrid/electric vehicle applications," 2011 IEEE Vehicle Power and Propulsion Conference, Chicago, IL, 2011, pp. 1-6.

[2] K. Shi, D. Zhang and Y. Gu, "Interleaved Current-Driven Phase-Shift Full-Bridge Converter With Magnetic Integration and Voltage Doubler Rectifiers," in IEEE Transactions on Power Electronics, vol. 33, no. 10, pp. 8308-8321, Oct. 2018.

[3] S. Kim, A. M. Naradhipa and S. Choi, "Development of a High Power Density GaN-based Transistor Low-Voltage High-Current Phase-Shift Full-Bridge Current Doubler Converter for Electric Vehicles," 2019 IEEE Energy Conversion Congress and Exposition (ECCE), Baltimore, MD, USA, 2019, pp. 1364-1369.